Generated using the official AMS LaTeX template v6.1

# Resolution-Dependence of Extreme Wind Speed Projections in the Great Lakes Region

Michael Morris, [a] Paul J. Kushner,[a] G.W.K. Moore,[a, b] , and Oya Mercan[c]

[a] *Department of Physics, University of Toronto*

[b] *Department of Physical and Chemical Sciences, University of Toronto Mississauga*

[c] *Department of Civil and Mineral Engineering, University of Toronto*

*Corresponding author*: Michael Morris, michaelobrien.morris@mail.utoronto.ca

ABSTRACT: The effect of anthropogenic climate change on extreme near-surface wind speeds is uncertain. Observed trends are weak and difficult to disentangle from internal variability, and model projections disagree on the sign and magnitude of trends. Standard coarse-resolution climate models do not represent fine structures of relevant physical phenomena such as extratropical cyclones (ETCs), upper-level jet streaks, surface energy fluxes, and land surface variability as well as their high-resolution counterparts. Here we use simulations with the NCAR Community Earth System Model with both uniform (110 km) resolution and the variable resolution configuration (VR-CESM-SONT, 110 km to 7 km), to study the effect of refined spatial resolution on projections of extreme strong and weak wind speeds in the Great Lakes region under end-of-century RCP8.5 forcing. The variable-resolution configuration projects strengthening of strong-wind events in the refined region with the opposite occurring in the uniform-resolution simulation. The two configurations provide consistent changes to synoptic scale circulations associated with high-wind events. However, only the variable resolution configuration projects weaker static stability, enhanced turbulent vertical mixing, and consequentially enhanced surface wind speeds, because boundary layer dynamics are better captured in the refined region. Both models project increased frequency of extreme weak winds, though only VR-CESM-SONT resolves the cold-season inversions and summertime high temperatures associated with stagnant wind events. The identifiable mechanism of the changes to strong winds in VR-CESM-SONT provides confidence in its projections and demonstrates the value of enhanced spatial resolution for the study of extreme winds under climate change.

SIGNIFICANCE STATEMENT: In this study we compare climate change projections of high and low extreme wind speeds in the Great Lakes region between a standard coarse-resolution simulation and a high-resolution simulation performed using the same climate model. The fine-resolution simulation projects strengthening high wind speeds, opposite to the coarse-resolution simulation. Both project increasing frequency of extreme weak winds, but the human-health related impacts of stagnant winds are only captured at fine-resolution. The changes in the coarse-resolution simulation are explained by changes to large-scale circulation, while the fine-resolution changes are linked to local processes the coarse model does not resolve. This helps explain the diverging projections of strong winds and gives greater credibility to the fine-resolution simulation.

## 1. Introduction

Extreme high winds pose a threat to the construction (Schuldt et al. 2021) and wind-power (Pryor et al. 2020) industries, as well as homes (Sandink et al. 2019) and human lives (Ashley and Black 2008). In the Great Lakes region, extreme winds have been linked to ecological damage and poor water quality (Jabbari et al. 2021). On the opposite end of the wind speed distribution, extreme stagnant winds, especially in urban regions, are linked to poor air quality (Garrido-Perez et al. 2018; Dempsey 2018; Hsu and Cheng 2019) and extreme high temperatures (Javanroodi and Nik 2020). Stagnating winds also reduce the energy resources available to the wind-power industry (Zeng et al. 2019; Pryor et al. 2020). Changes to extreme weather under climate change is a topic of high interest due to these impacts on infrastructure, industry, and human health and safety. The sixth IPCC Assessment Report (Seneviratne et al. 2023) concluded that that anthropogenic emissions have led to increased frequency and intensity of weather and climate extremes. However, most of the work to date on extreme weather has focused on temperature and precipitation, with the previous IPCC Assessment Reports not discussing changes to extreme wind speeds outside of the context of other phenomena like tropical cyclones. Changes to extreme high or low wind speeds under climate change could elevate the severity of their associated hazards, so understanding these changes is critical for climate change adaptation and planning.

Unfortunately, the effect of climate change on extreme wind speeds is uncertain. A synthesis of studies on observed wind speed trends identified an overall “global stilling” over land

(McVicar et al. 2012) during the late 20th century, though recent work has identified a reversal in this trend (Zeng et al. 2019). In either case, the changes are difficult to disentangle from internal variability (Zha et al. 2021), so detecting a climate change signal has proven difficult. Future projections of extreme strong wind speeds are also uncertain. The spatial resolution of the global climate models used to make projections is typically too coarse to directly simulate extreme high wind speeds and gusts (Skamarock 2004; Larsén et al. 2012), making model output difficult to evaluate without post-processing such as statistical downscaling. However, even different regional climate models (RCMs) with higher spatial resolution can produce changes of opposite sign (Pryor et al. 2012; Jeong and Sushama 2019), though the resolution of models in these studies (approx. 50 km) is still too coarse to reliably simulate extreme winds (Larsén et al. 2012).

Limited-area regional models can suffer from artefacts relating to incompatibility between the specified boundary conditions and RCM physics, namely "chaotic divergence" and "upscale influence" (Scinocca et al. 2016). To avoid these technical issues, we use the variable resolution configuration of the NCAR Community Earth System Model, VR-CESM (Gettelman et al. 2018), to produce dynamically downscaled climate change projections of extreme wind speeds. In VR-CESM, a high-resolution grid covering a limited region is nested inside of a global coarse resolution grid. Information flows both into and out of the high-resolution domain, ensuring consistency between the global and regional climate. This methodology also allows for isolation of the effects of refined resolution on the results, through comparison with output from the same model, with the same physics, but with a uniform coarse grid. Wang et al. (2018, 2020) used VR-CESM with refined resolution over California to study the effect of climate change on wind speed primarily for wind energy applications. We build on this work by considering changes to extreme wind speeds in the eastern Great Lakes region of North America. This region was selected in part due to its high population and population density (US EPA 2015), meaning the impacts of any potential changes would affect a large number of people. It was also chosen for consistency with Morris et al. (2023), which investigated large-scale drivers of extreme strong wind events in this region under historical climate conditions. Investigating projections of extreme winds in this region under future climate is a natural progression of our previous work.

The reasons for the aforementioned model disagreement regarding future extreme winds are not well understood, indicating a lack of process understanding regarding the physical causes for potential changes. Extreme wind events in the northern hemisphere midlatitudes are often driven by synoptic-scale phenomena such as extratropical cyclones (ETCs) and upper-level jet streaks which are resolved by coarse resolution models (Morris et al. 2023), but changes to the storm tracks and jet stream are controlled by multiple opposing processes leading to uncertainty (Shaw et al. 2016). Decreased baroclinicity may reduce the frequency and intensity of ETCs, but thermodynamic effects of increasing atmospheric moisture may increase cyclone intensity and associated wind speeds (Sinclair et al. 2020; Priestley and Catto 2022). One region where there is a clear projected climate change signal related to strong wind extremes is the Arctic. Mioduszewski et al. (2018) found large increases to mean and extreme Arctic wind speeds due to sea ice loss and resulting decreases to surface roughness and static stability. Like that work, we aim to identify physical mechanisms that explain projected changes to extreme wind speeds in our study region. Morris et al. (2023) showed that VR-CESM improves representation of both the spatial structure and intensity of ETCs and jet streaks associated with high wind events as well as the strength of vertical coupling between upper-level jet streaks and strong near-surface winds. These results demonstrate the utility of VR-CESM for process-related investigation of changes to extreme winds.

The purpose of this study is therefore to investigate and explain the climate change signal for both strong and weak extreme wind events in the eastern Great Lakes region, and identify the value added by the refined spatial resolution of VR-CESM relative to global coarse resolution simulations, bearing in mind the significant computational cost of refined resolution (Morris et al. 2023). Following previous work, the primary focus will be on strong wind extremes, but we also consider stagnant wind events due to their important societal impacts and the widely reported trend of global terrestrial stilling. Expanding on Morris et al. (2023), we analyze the effect of refined spatial resolution on the near-surface wind speed itself as well as changes to both synoptic-scale and local-scale processes that cause extreme wind speeds. The results will show disagreement in the sign of the change of extreme high wind speeds over land, and identifying a physical explanation for this disagreement is a key contribution of this work.

This paper is organized in the following manner: Section 2 will provide further details on the CESM simulations used to study extreme wind speeds and the impact of regionally refined resolution, and the analysis methods applied to the model output. Section 3 will present the results, first on extreme high wind speeds and then regarding extreme stagnant winds. Finally, Section 4 will summarize and discuss the major findings and conclusions.

## 2. Data & Methods

### *a. Climate Model Simulations*

The climate model used for this work is CESM version 2.1.0 (Hurrell et al. 2013). We run 30-year long "time-slice" simulations that actively simulate the atmosphere (CAM5, Neale et al. (2012)) and land (CLM5, Lawrence et al. (2019)) components, and we prescribe monthly sea surface temperatures (SST) and sea ice concentration (SIC) as annually repeating boundary conditions. Lake temperatures are actively simulated by the land model and are therefore not prescribed. Each year of simulation requires approximately 18000 core-hours (Morris et al. 2023). For this type of simulation, each year represents a sample of atmosphere-land internal variability under the prescribed forcing. Typical 2000s conditions are used as the historical baseline using the default F2000C5 component set, but with SST and SIC taken from the CESM1 Large Ensemble (Kay et al. 2015) 1990–2010 monthly climatology. Concentrations of atmospheric constituents such as greenhouse gases and aerosols are set to year 2000 values. The 2000s-forcing simulations were previously used by Morris et al. (2023) to characterize large-scale drivers of extreme wind events under historical climate conditions. For the climate change simulation, we use end-of-century RCP8.5 forcing to maximize the signal to noise ratio. SSTs and SIC are prescribed using the CESM1-LE 2080–2100 monthly climatology, with GHG and aerosol concentrations set to year 2090 RCP8.5 values. As such, we refer to these as 2090s-forcing simulations. For each case, a mid-monthly adjustment is applied to the SST and SIC boundary conditions using the NCAR *bcgen* software to ensure the model computed monthly means are consistent with the boundary conditions (CSEG 2013). The computations were performed on the Niagara cluster at the University of Toronto's Scinet HPC facility (Loken et al. 2010; Ponce et al. 2019).

To study the effect of refined spatial resolution on near-surface wind speeds, we compare results from VR-CESM to output from simulations with identical boundary conditions and a uniform coarse-resolution (110 km) grid. The coarse-resolution is much less computationally expensive, with each year requiring about 1200 core-hours (Morris et al. 2023). Grids for the two simulations are shown in Figure 1. Our VR-CESM simulation (referred to as VR-CESM-SONT) has highest resolution over southern Ontario, Canada, with the grid cell size decreasing from 110 km ($\sim 1°$) over most of the globe to $\sim$ 7 km over a $5° \times 5°$ region centred at 43.3°N, 83.2° W. The grid refines gradually over three nested regions of intermediate resolution, with the grid cell size shrinking by a factor of 2 over each transition. The atmosphere model in VR-CESM employs the spectral element dynamical core (CAM-SE, Dennis et al. (2012)) with a cubed-sphere grid for spatial discretization, which allows for the regionally refined spatial resolution. For consistency, we also use CAM-SE for the coarse resolution simulation (following Zarzycki et al. (2015)), and refer to it hereafter as CESM-SE-UNIF. To satisfy the Courant–Friedrichs–Lewy constraint, the physics time step for VR-CESM-SONT is reduced from 1800 s (for global 110 km resolution) to 450 s. Regional refinement does not have a substantial effect on global-scale climate, as the global mean surface air temperature changes for each model configuration (2090s minus 2000s) differ by less than 0.1°C (3.19°C for VR-CESM-SONT versus 3.24°C for CESM-SE-UNIF).

The following output variables were archived from each simulation at 4-hourly instantaneous sampling and are used for analysis of extreme wind speed events: 10 m wind speed, turbulent wind gust magnitude, sea level pressure (SLP), surface pressure (PS), and temperature, zonal wind, and meridional wind on 30 hybrid-sigma vertical levels. PS is used for interpolating the data on model levels onto pressure levels. Surface turbulent sensible heat flux was not initially archived at high frequency, so the simulations were re-run to obtain this variable. The re-run simulations had no meaningful differences from the initial runs, other than the transient sequencing of internal variability due to the chaotic nature of the climate system.

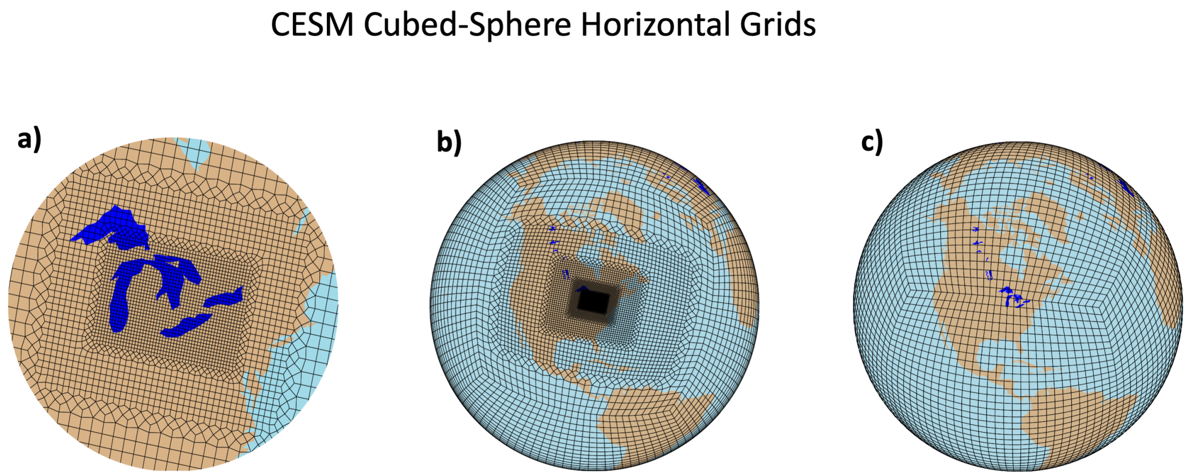


FIG. 1. (a) Refined grid for the 14 km and 7 km resolution regions for VR-CESM-SONT, and global cubed-sphere grids for b) VR-CESM-SONT and c) CESM-SE-UNIF, the two climate model simulations used in this study. The grid for VR-CESM-SONT is rotated with respect to the default configuration of the CESM-SE-UNIF grid, to place the entire refined area on one cube face. Refinement regions that overlap the transition between faces of the cubed sphere can lead to numerical instability and are recommended against by the VR-CESM developers.

### *b. Analysis Methods*

#### 1) Extreme Event Selection

Extreme events in each simulation are identified using the peaks-over-threshold method, using a grid cell's 98$^{th}$ percentile wind speed (hereafter shortened as $U_{98p}$) as the lower bound for extreme strong wind events, and the 5$^{th}$ percentile as the upper bound for extreme stagnant wind events. $U_{98p}$ has been used as a threshold for identifying extreme high wind events in many previous works (Hanley and Caballero 2012; Welker and Martius 2015; Lukens et al. 2018; Morris et al. 2023), and has the benefit of providing a large sample size that can be used to characterize dynamical drivers (Sillmann et al. 2017; Morris et al. 2023). Using a higher threshold like the 50-year return period wind speed ($U_{50}$) would connect more directly to damaging impacts, but much longer simulations would be required to produce a sufficient sample of events with wind speed at or above $U_{50}$. The high computational cost of high-resolution climate simulation makes this unfeasible. To ensure the events represent extremes over an extended region we select those for which 25% of the area in the 7 km resolution domain meet the wind speed threshold. This area threshold is why the 5$^{th}$ percentile is used instead of the 2$^{nd}$ percentile for the stagnant wind events. For the 2000s VR-CESM-SONT case, only 43 bottom-2 percentile events meet the area threshold, which is a very small sample size when compared to 426 top-2 percentile events and 960 bottom-5 percentile events. To ensure the events are statistically independent, we discard events which occur within 24 h of another, retaining the timestamp with the strongest region-averaged wind speed for high wind events, and the lowest region-averaged wind speed for stagnant wind events. Since few strong wind events occur in the summer in the study region and events in this season show qualitatively different large-scale characteristics (Morris et al. 2023), we restrict the analysis of strong winds to the DJF, MAM, and SON seasons (September to May). Events at any time of year are included in the analysis of stagnant winds.

#### 2) Composite Analysis

We study both synoptic-scale and local-scale meteorological drivers of extreme high and low wind speed events by producing composite average maps of related climatic variables during extreme wind events. Before compositing, strong-wind events are separated by the quadrant of the region-averaged wind direction, calculated using the lowest model level meridional and zonal wind components averaged over the region with 7 km resolution in VR-CESM-SONT. This is done because Morris et al. (2023) found that extreme high-wind events in the study region show markedly different large-scale SLP and 300 hPa wind patterns for events with northeasterly (NE), southeasterly (SE), northwesterly (NW), and southwesterly (SW) wind direction. We also find that the climate change response of extreme high near-surface winds and variables associated with driving processes differ for events with different wind direction. The composite patterns for weak-wind events do not show the same wind-direction dependence, so these events are not separated by wind direction before compositing.

Like Morris et al. (2023) we study large-scale drivers of extreme wind events by compositing SLP and 300 hPa winds. SLP used to identify relevant circulations in the lower troposphere, like ETCs for extreme high winds (Letson et al. 2021) and anticyclones for stagnant winds (Hsu and Cheng 2019). Winds at 300 hPa identify upper-level jet streaks (Uccellini and Kocin 1987; Trier et al. 2020) which are associated with strong ETCs and surface winds, and possibly blocking, which is connected to stagnant winds (Dempsey 2018; Garrido-Perez et al. 2018). We expand on the previous work by also considering a local-scale driver of extreme near-surface winds, namely static stability in the atmospheric boundary layer. Static stability, which is analyzed for both weak and strong wind extremes, is calculated between the two lowest model hybrid-sigma levels using the following equation:

$$s = -\frac{T}{\theta}\frac{\partial \theta}{\partial p} \tag{1}$$

Or, in terms of finite differences of model output variables,

$$s = -T \times \left[ \frac{ln(T_1) - ln(T_2)}{p_1 - p_2} - \frac{R/c_p}{p_1} \right] \tag{2}$$

Where $s$ is the static stability, $T$ is the temperature, $\theta$ is the potential temperature, $R$ is the gas constant for dry air, $c_p$ is the specific heat capacity at constant pressure, and subscripts 1 and 2 refer to quantities on the lowest and second lowest model vertical levels. Low (high) static stability is associated with stronger (weaker) near-surface wind speed since lower (higher) stability leads to increased (reduced) mixing of high-momentum air from the lower troposphere into the boundary layer (Mioduszewski et al. 2018). The CESM diagnostic WGUSTD (described as ”wind gusts from turbulence” in the output files) is used to quantify the degree of vertical mixing of momentum, since it is derived from a turbulent perturbation vertical velocity (Bretherton and Park 2009). Boundary layer stability is strongly controlled by turbulent fluxes of heat from the surface, so we produce composites of SHFLX (turbulent sensible heat flux).

### 3) Climate Change Signals & Statistical Significance

Responses to anthropogenic climate change are generally quantified by subtracting the results of the 2000s-forcing control simulations from the 2090s-forcing simulations. Because these are time-slice simulations representing two fixed periods, neither trends nor changes per degree of warming can be calculated. We identify mechanisms for the changes to extreme wind speeds by calculating changes to the composite patterns associated with the physical process under investigation - cyclones, jet streaks, blocking, and boundary layer stability.

Statistical significance of climate changes to the composites is assessed using a two-sample Welch's $t$-test (Welch 1938), which does not assume equal variance between the two samples. Variances are calculated across the events contributing to the composite mean. The same test is used when assessing the significance of composite anomalies from the climatology. To construct climatological means from which to calculate anomalies and climatological variances for significance testing, we calculate a weighted average of the DJF, MAM, and SON seasonal means/variances where the weights are the number of extreme events which occur in each season. Because significance tests are performed for many grid cells, we control for the False Discovery Rate (FDR) following Wilks (2016). Using this method, the $N$ $p$-values from the grid cell-wise $t$-tests (where $N$ is the number of grid cells) are sorted in increasing order and indexed using order statistic notation $p_{(1)}, ..., p_{(N)}$. A new, more stringent significance threshold $p_{FDR}$ is calculated using the following formula:

$$p_{FDR} = \max_{i=1,...,N} \left[ p_{(i)} : p_{(i)} \leq (i/N)\,\alpha \right] \tag{3}$$

Where $\alpha$ is the significance threshold for the original hypothesis test (i.e. $\alpha = 0.05$, 0.1, etc.). In the final analysis, $t$-tests for which $p < p_{FDR}$ are considered statistically significant. Further explanation of the FDR method can be found in Wilks (2016).

The $t$-test is not appropriate for assessing significance of changes to quantiles, so a bootstrap resampling procedure is used to assess significance of changes to $U_{98p}$. We calculate $U_{98p}$ for each resampling iteration, and the 2.5$^{\text{th}}$ and 97.5$^{\text{th}}$ percentiles of the distribution across iterations are used directly to assess significance. The same procedure is used to test significance of changes to the 50-year return period wind speed in Section 3.b.5.

## 3. Results

### *a. Changes to 10 m Wind Speed*

We assess changes to extreme high wind speeds in the study region by calculating the change to $U_{98p}$ at each grid cell. Figure 2 shows the September–May $U_{98p}$ for the 2000s-forcing simulations, and the 2090s RCP8.5 climate change signal, expressed as a percentage change. The high resolution of VR-CESM-SONT allows it to capture the contrast in wind speeds between the land and lakes, with higher wind speeds over the smoother water surface. The coarse resolution model, CESM-SE-UNIF, shows some evidence of enhanced wind speeds over the lake areas but the contrast is not as strong in magnitude nor are the spatial boundaries as sharp. Away from the lakes, the $U_{98p}$ for VR-CESM-SONT is mostly weaker than in CESM-SE-UNIF and the difference is statistically significant. This is possibly due to finer representation of complex topography (Supplemental Figure 1) in the Allegheny Plateau to the southwest of Lake Erie, and the Opeongo Hills to the north of Lake Ontario, as these regions are where $U_{98p}$ is lowest in both simulations.

The change to $U_{98p}$ under elevated climate forcing is the key result from Figure 2. While CESM-SE-UNIF projects statistically significant weakening to extreme high wind speeds over most of the study region, VR-CESM-SONT projects significant strengthening over land, and weakening over Lakes Ontario and Erie. The two models disagree regarding the sign of the change nearly everywhere in the domain over land. Simulations with 2040s forcing (i.e. SST and SIC from the CESM1-LE 2030-2050 ensemble mean monthly climatology and year 2040 RCP8.5 radiative forcing) show similar spatial patterns but with changes of weaker magnitude and smaller areas of statistically significant changes over land (Supplemental Figure 2), demonstrating the robustness of these patterns of change to $U_{98p}$ in each model configuration. Much of the forthcoming discussion of extreme high winds attempts to identify the different mechanisms for the changes in each model to explain the resolution sensitivity of the $U_{98p}$ projections, using the 2090s simulations as the future projection period.

Before discussion of the mechanisms of the changes to extreme high winds, we present in Figure 3 the region-averaged changes to different percentiles of the 10 m wind speed distribution. This

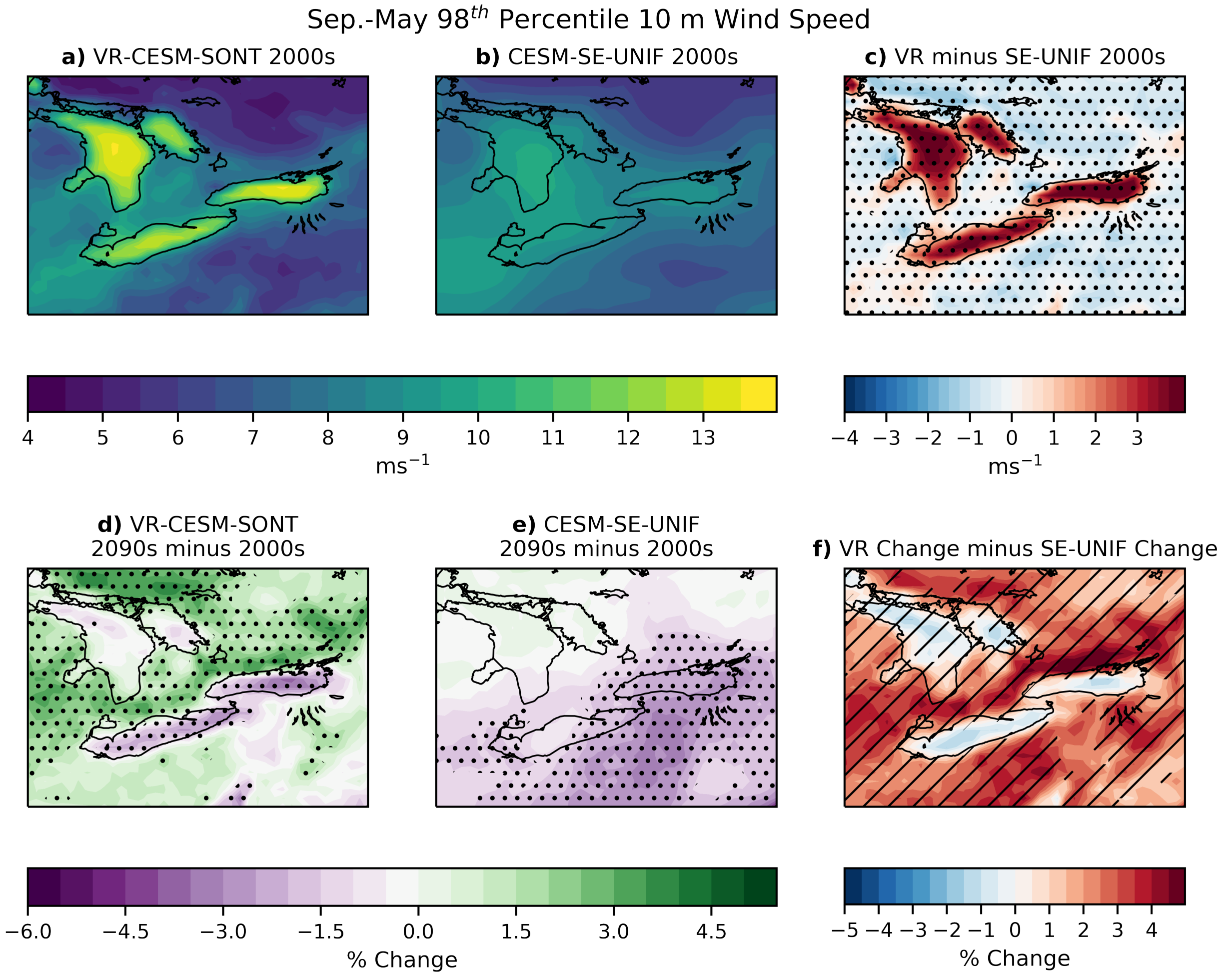


FIG. 2. (a)-(b): 98th percentile wind speed during the September–May season from the 2000s forcing simulations for VR-CESM-SONT and CESM-SE-UNIF. Panel (c) is the difference between (a) and (b). Stippling indicates statistically significant difference between the two simulations. (d)-(e): Percent change to the 98th percentile wind speed from the 2000s to 2090s under RCP8.5 forcing, for VR-CESM-SONT and CESM-SE-UNIF. Stippling shows where the change is significant at the 5% level, per the bootstrap resampling test described in Section 2.b.3. Panel (f) shows the difference between the climate change signals for the two simulations. The hatching indicates where the simulations disagree on the sign of the change.

allows us to answer an important question about the statistical nature of the projected changes — are they primarily due to a shift in the distribution (i.e. a change in the mean), or a change in shape of the distribution (i.e. a change in variance/skewness)? This figure shows that the increasing extreme high wind speeds in VR-CESM-SONT are mainly due to an increase in variance of the

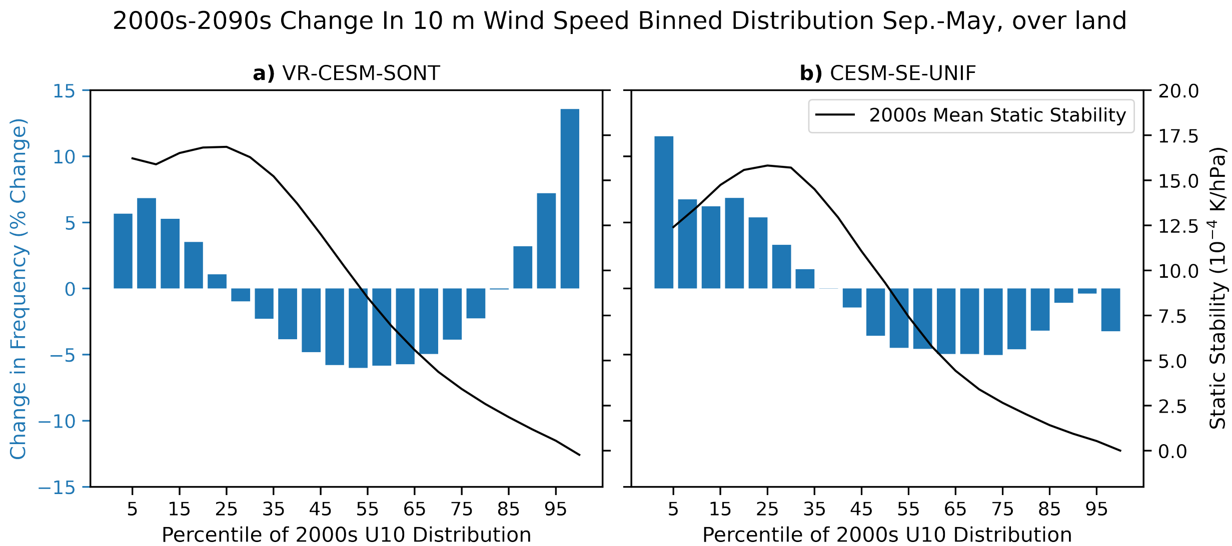


FIG. 3. Projected 2000s to 2090s change to September–May 10 m wind speed distributions in VR-CESM-SONT (a) and CESM-SE-UNIF (b), expressed as percentage changes to the frequency of occurrence for wind speeds in each 5-percentile bin of the 2000s distribution. Separate histograms were calculated for each land grid cell in the study region, and averaged to produce the results shown. The black line is the region-averaged static stability for times in the 2000s simulation with wind speeds in each bin, calculated between the two lowest model vertical levels. This style of plot was inspired by Mioduszewski et al. (2018).

wind speed distribution, with wind speeds in both high and low tails of the distribution occurring more frequently. CESM-SE-UNIF shows, to first order, a shift in the mean wind speed. Both simulations project increasing frequency of extreme weak winds, albeit for different reasons, which is what motivated the investigation of these events in Section 3.c. The black curves in this figure, which represent 2000s-forcing (control-run) static stability values for events with wind speeds in the corresponding percentile bin, prove that extreme high 10 m winds are associated with a less stable boundary layer, and weaker winds are associated with higher static stability. This encourages investigation of changes to local static stability during extreme wind events, in addition to the large-scale circulation patterns associated with extreme winds identified in the predecessor study Morris et al. (2023) such as ETCs and upper-level jet streaks. Possible increases to blocking and stability will be investigated as a mechanism for increases to extreme stagnant winds.

### *b. Strong Wind Events*

#### 1) 10 m Wind Composites

Composites of the 10 m wind speed and wind vectors on the lowest model level for the 2000s simulations are shown in Figure 4a-d. As mentioned in Section 2.b.2, we separate extreme high wind events by the quadrant of the region-averaged wind direction. For conciseness we show only the NW and SW quadrants, since westerly winds comprise the overwhelming majority of extreme high wind events in the Great Lakes region. Like Figure 2a, the VR-CESM-SONT 2000s composites show sharp contrast between wind speed over the land and lakes, which exists but is less sharp in CESM-SE-UNIF. Percent changes between the control and future period are shown Figure 4e-h. The only event class which shows significant changes is SW events in VR-CESM-SONT, and the spatial pattern of changes for this quadrant matches the $U_{98_p}$ change for this model (Fig. 2d). VR-CESM-SONT also projects that SW extreme high winds will occur more frequently, suggesting that the changes to $U_{98_p}$ are primarily due to changes to SW strong winds.

#### 2) Large-Scale Drivers of Strong Winds

Morris et al. (2023) identified ETCs, diagnosed by deep minima in SLP anomaly fields, as a key synoptic-scale driver of extreme near-surface wind speeds. SLP anomaly composites for the 2000s extreme high winds are presented in Figures 5(a-d) and Figure 6(a)-(d). They show statistically significant anomalies which indicate the presence of an intense ETC below an upper-level jet streak. These are similar to the composites from these simulations in Figures 8 and 10 of Morris et al. (2023), only for extreme winds over a larger region instead of at a single location near Toronto. The changes to the composite SLP anomalies and jet streaks are shown in Figures 5(e)-(f) and 6(e)-(f) respectively. Both models project non-significant weakening of the SLP minima and some significant weakening to the jet streak wind speed. Since deeper SLP minima and stronger upper-level jet streaks are associated with stronger wind speeds (Morris et al. 2023), the changes to the composite large-scale circulations in VR-CESM-SONT are not consistent with stronger near-surface winds. Therefore the $U_{98_p}$ increases in VR-CESM-SONT cannot be explained by changes to ETC or jet streak intensity. The weaker SLP anomalies and weaker upper-level jet streak wind speeds in CESM-SE-UNIF are consistent with its projection of weaker extreme wind

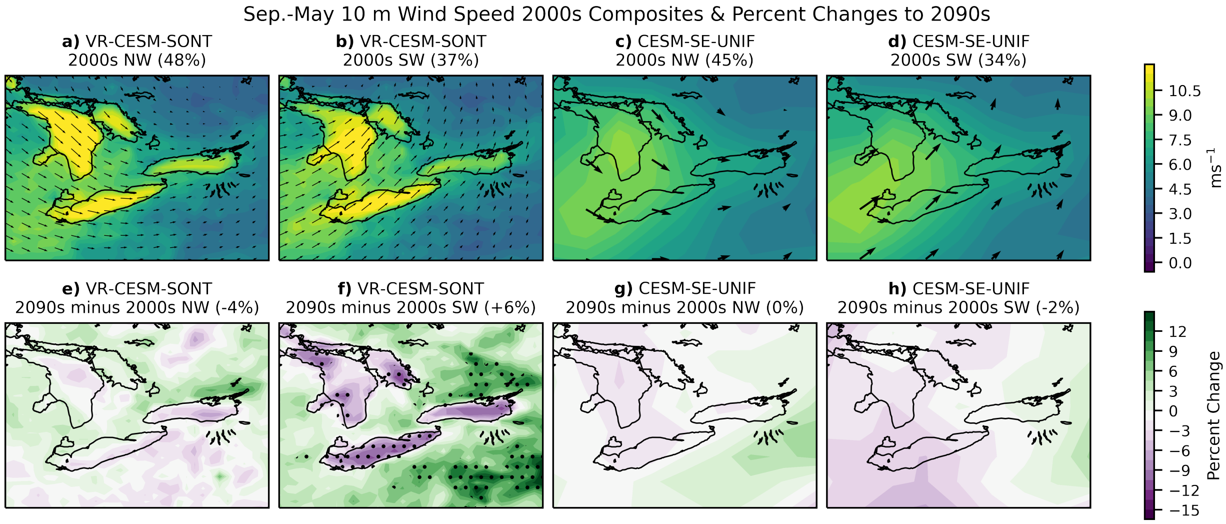


FIG. 4. (a)-(d): Composites of 2000s-period 10 m wind speed (filled contours) and lowest model level wind components (vectors) for NW and SW extreme high wind events in VR-CESM-SONT and CESM-SE-UNIF. Percentages in the subplot titles indicate the proportion of extreme high wind events with wind direction in that quadrant. (e)-(h): Differences between 2090s and 2000s 10 m wind speed composites, expressed as percentage changes. Percentages in the subplot titles indicate the change in proportion of extreme events in that quadrant. Stippling indicates where changes are significant at the 10% level, assessed via a Welch's *t*-test as described in Section 2.b.3.

speeds, suggesting that at coarse-resolution, changes to surface wind extremes are more strongly linked to changes in the large-scale circulation than at fine resolution.

### 3) Local-Scale Drivers of Strong Winds

Having ruled out changes to large-scale circulation patterns as the physical mechanism responsible for increasing extreme wind speeds over land in VR-CESM-SONT, we look to boundary layer stability for an alternate explanation. Over land, composites of static stability for strong wind events (Fig. 7a-d) show negative anomalies, consistent with Figure 3, which showed that weaker static stability is associated with stronger wind speeds in both model configurations. The SW events in VR-CESM-SONT have anomalously high stability over the lakes, and this pattern is amplified by the climate change signal (Fig. 7f). CESM-SE-UNIF shows weaker negative anomalies near the lakes, but the spatial resolution appears to be too coarse to fully resolve the the land-lake contrast.

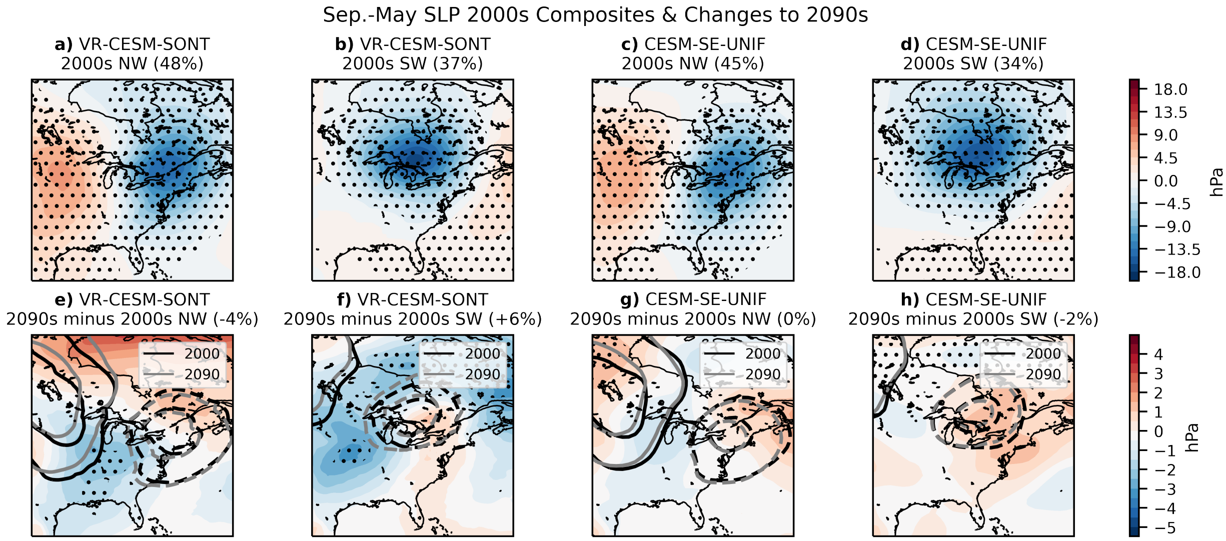


FIG. 5. As in Figure 4, but for SLP anomaly composites. The spatial domain of the plot is larger in order to show the relevant SLP anomaly pattern, which has a larger characteristic spatial scale than the extreme wind speeds. Stippling in the panels (a)-(d) shows where the anomalies are significantly different from the 2000s climatological mean at the 5% level, as described in Section 2.b.3. Stippling in (e)-(h) indicates where the difference between the 2000s and 2090s composites is significant at the 10% level. Black contours show the 2000s SLP anomaly composite, and grey contours are the same but for the 2090s composites. Percentages in the subplot titles have the same meaning as Figure 4.

The spatial pattern of the VR-CESM-SONT static stability change for SW events is consistent with the changes to 10 m wind speed; the wind speed weakens over the lakes where stability increases, and strengthens over land where stability decreases. The high magnitude of the spatial correlation between the changes to 10 m wind speed and static stability for the SW events ($r = -0.76$) provides evidence that changes to boundary layer stability are responsible for the changes to $U_{98p}$ in VR-CESM-SONT. The only other high-wind event regime which shows a significant change to static stability under 2090s forcing is the SW quadrant for CESM-SE-UNIF, and this region of decreasing stability shows weak increases in the 10 m wind speed composite (Fig. 4h). Neither of the simulations show significant changes to static stability or to 10 m wind speed for events with wind direction in the other quadrants.

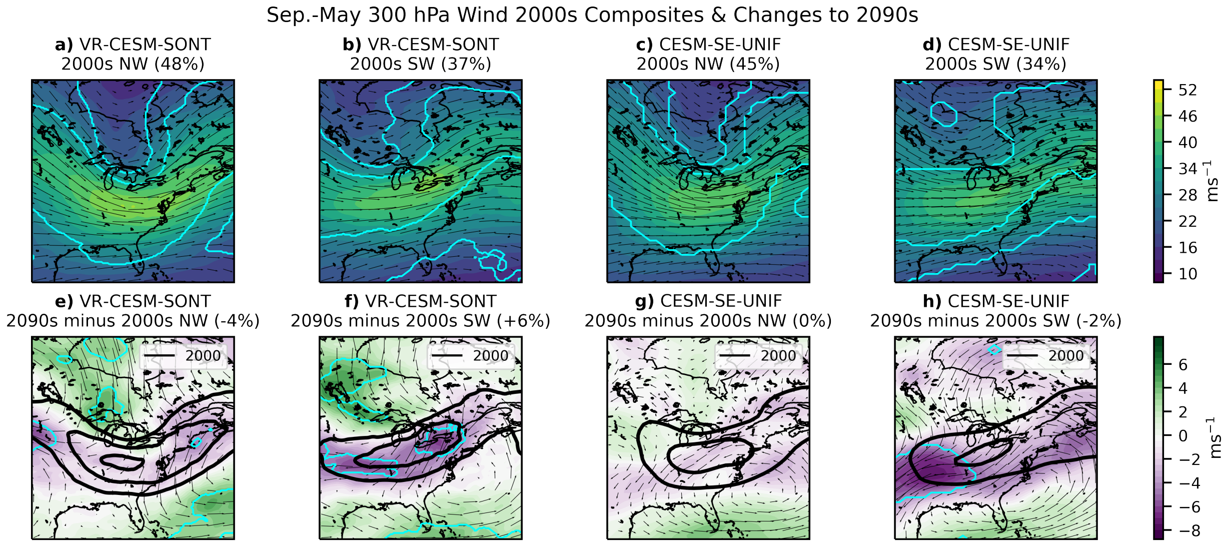


FIG. 6. As in Figure 4, but for 300 hPa wind composites. The thin cyan contours in (a)-(d) outline regions where the 300 hPa wind speed differs significantly from the climatological mean at the 5% level, and where the climate change signal is siginificant at the 10% level in panels (e)-(h). The black contours in (e)-(h) are the 300hPa wind speed contours for the 2000s composites, similar to Figure 5.

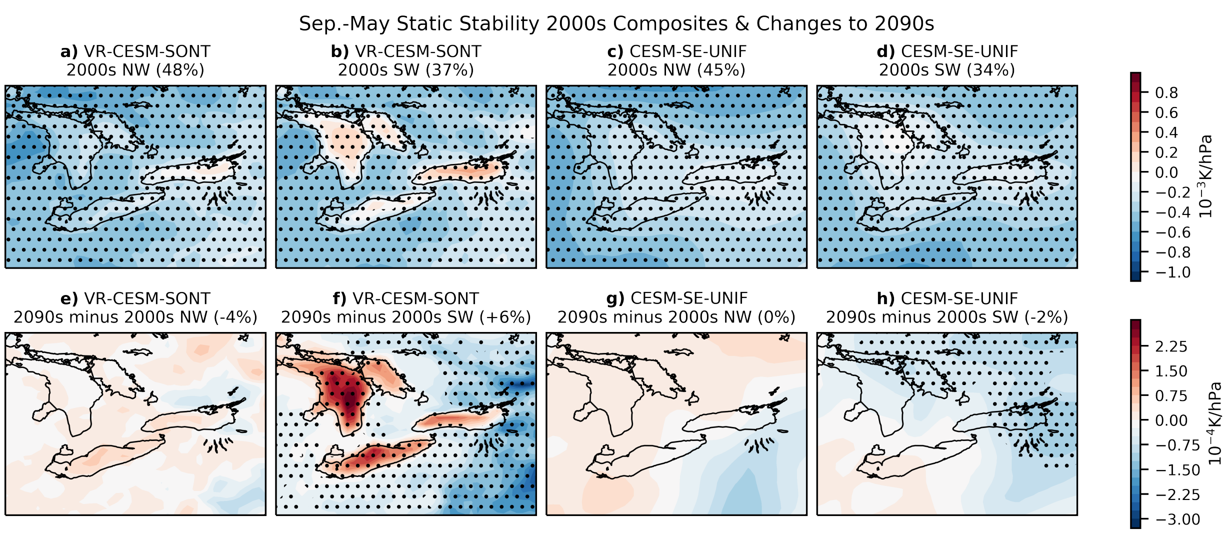


FIG. 7. As in Figure 4, but for anomalies of static stability between the two lowest model vertical levels. Stippling has the same meaning as in Figure 5.

To test whether reduced static stability is leading to stronger extreme high wind speeds, we composite the CESM turbulent vertical velocity output parameter (WGUSTD) described

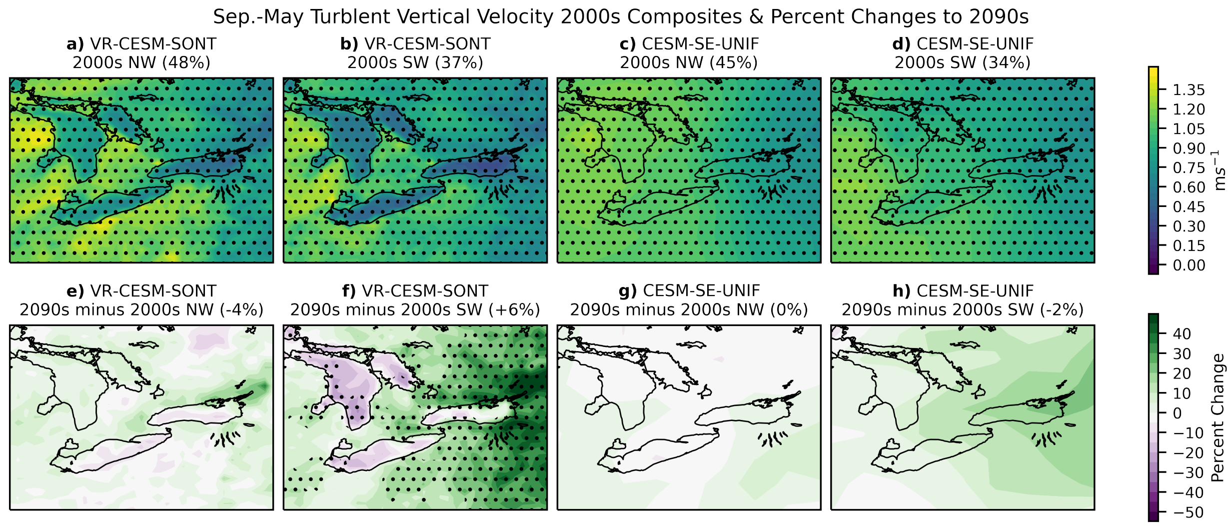


FIG. 8. As in Figure 7, but for the CESM turbulent vertical velocity parameter.

in Section 2.b.2 (Fig. 8). The 2000s composites show weaker turbulence over the lakes, where static stability is high, than over land, where static stability is anomalously low. Again, the only regime which shows significant changes is VR-CESM-SONT SW events, and the changes are highly correlated with the changes to static stability ($r = -0.84$) and wind speed ($r = 0.76$). By visual inspection of the VR-CESM-SONT SW composites in Figures 4, 7 and 8, the largest changes to stability and WGUSTD all occur in the eastern part of the study domain, and they all have opposite responses to climate change forcing over the land and the lakes. These results suggest a strong link between static stability and vertical mixing of momentum into the boundary layer, which contributes to strong near-surface wind speeds over land.

To test quantitatively that the changes to strong wind speeds in CESM-SE-UNIF are more strongly controlled by large-scale circulation, and the changes in VR-CESM-SONT are more strongly controlled by reduced local static stability, we propose the following multiple linear regression model:

$$\overline{U}_{10m} \sim \beta_0 + \beta_1 \times SLP_{min} + \beta_2 \times \overline{s} \tag{4}$$

Where $\overline{U}_{10m}$ is the region-averaged 10 m wind speed over land, $SLP_{min}$ is the minimum sea level pressure within a 5° radius of the centre of the study domain, and $\overline{s}$ is the region-averaged static stability over land. We use the data for the 2000s simulations to estimate the coefficients $\beta_i$. Coefficient values and the goodness-of-fit statistic $R^2$ for the regression models are presented in Supplemental Table 1. We note that this model is not designed to make full predictions of wind speed, instead we use it for inference regarding the effect of changes to SLP versus static stability. For this reason it has only two explanatory variables, but of course there are many more factors that influence wind speed. This is particularly true for VR-CESM-SONT which is capable of resolving complex processes at finer spatial scales that a linear statistical model cannot hope to capture.

For each model configuration we calculate an expected change in $\overline{U}_{10m}$ due to each explanatory variable using the following procedure: we set the values of $SLP_{min}$ and $\overline{s}$ to those for the 2000s SW composite to produce a baseline value of $\overline{U}_{10m}$. Then we set $SLP_{min}$ equal to the 2000s composite value and $\overline{s}$ to the 2090s composite value to produce an expected future $\overline{U}_{10m}$ associated with the change in static stability, and finally we set $SLP_{min}$ to the 2090s composite value and $\overline{s}$ to the 2000s composite value to produce an expected future $\overline{U}_{10m}$ associated with the change in SLP. For VR-CESM-SONT (CESM-SE-UNIF), the "true" projected change in $\overline{U}_{10m}$ for SW events is +3.34% (-1.66%), the expected change due to the change in static stability is +1.22% (+0.66%), and the expected change due to the change in SLP is -0.93% (-1.32%). The linear regression model supports our hypothesis that the changes to strong wind extremes in the coarse resolution model are more strongly controlled by changes in the large-scale circulation because the estimated change due to SLP explains nearly 80% of the "true" change in CESM-SE-UNIF. The estimated changes to $\overline{U}_{10m}$ due to static stability in VR-CESM-SONT does not match the simulated change as closely, but the sign of the change due to the change in stability is consistent with the simulated change. The magnitude of the expected change due to SLP for VR-CESM-SONT is also smaller than its expected change due to static stability, supporting the hypothesis that strong winds in VR-CESM-SONT are more sensitive to changes to stability than large-scale circulation.

4) Mechanism of Stability Changes

If reduced stability over land (and increased stability over the lakes) is responsible for the changes to extreme high wind speeds in VR-CESM-SONT, then what is causing these changes to stability? Increased turbulent heat flux from the surface leads to decreased atmospheric stability (Mioduszewski et al. 2018), and indeed composites of turbulent sensible heat flux show strong positive anomalies over land during extreme high wind events. The climate change response for the VR-CESM-SONT SW events is very large, being as strong as or stronger than the control-period anomalies (Fig. 9). The sensible heat flux changes for this case are highly correlated to both the static stability changes ($r = -0.73$) and the 10 m wind speed changes ($r = 0.82$), providing further evidence of the connection between surface fluxes, stability, and high wind speeds. Contrast in the sign of the change to sensible heat flux between the land and lake surface could be due to the higher specific heat capacity of water, making the lakes warm less than the land surface. Historical surface temperature trends in the ERA5 reanalysis (Hersbach et al. 2020) for this region are generally only statistically significant over land, and the magnitude of the trends is close to zero and occasionally negative over the Great Lakes (Supplemental Figure 3), meaning these model projections are physically plausible. VR-CESM coupled with CLM has been shown to improve simulation of surface fluxes (Burakowski et al. 2019), which gives greater confidence in the results of VR-CESM-SONT.

Region-averaged vertical profiles of potential temperature over land (Figure 10) confirm that the instability during the high wind events is confined to the lowest parts of the atmosphere. This provides further evidence that the wind speed changes are controlled by forcing from the surface. Potential temperature increasing with pressure (decreasing with height) indicates instability. The SW events in VR-CESM-SONT have the largest increase to $\partial\theta/\partial p$ between the surface and lowest model level. Destabilization occurs for events in other quadrants and in CESM-SE-UNIF, but its lower magnitude is consistent with the non-significant changes to high wind speeds for these other cases.

In summary, the projections of extreme high wind speeds under end-of-century RCP8.5 simulations for VR-CESM-SONT, which has 7 km spatial resolution over the eastern Great Lakes

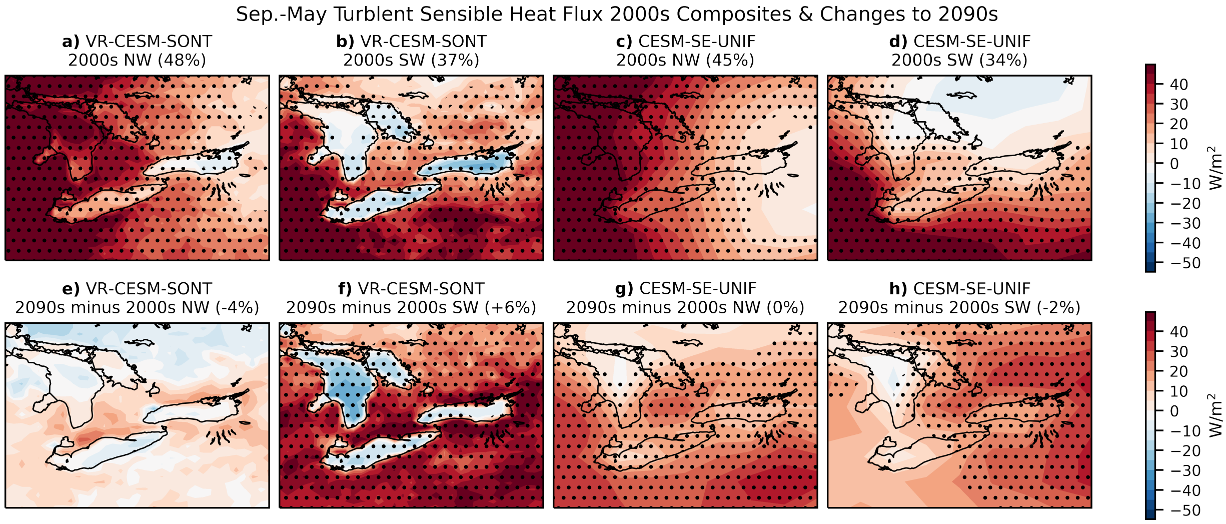


FIG. 9. As in Figure 7, but for anomalies of turbulent sensible heat flux. Positive indicates upward flux.

region, and CESM-SE-UNIF, which has 110 km resolution, have opposite sign over land in the study domain. The coarse resolution model projects weakening to $U_{98p}$ consistent with weaker large-scale circulation anomalies associated with top-2 percentile wind speed events. The fine-resolution model projects similar weakening to the large-scale circulation anomalies, but increasing extreme high wind speeds over land, predominantly in the SW quadrant of the wind rose (Fig. 4). VR-CESM-SONT projects weaker strong winds over the lakes, but the projections over both land and the lakes appear to be driven by changes to boundary layer stability (Fig. 7) caused by changes to surface heat flux (Fig. 9). The destabilization leads to increased turbulent vertical velocity (Fig. 8), and thus increased mixing of high momentum air from the lower troposphere into the boundary layer. The coarse spatial resolution of CESM-SE-UNIF is evidently too coarse to capture these turbulent effects, which is why its changes to extreme high wind speed are instead controlled by the synoptic-scale circulation changes.

### 5) Impacts of Extreme Strong Winds

One important hazard posed by extreme strong wind speeds is damage to buildings, especially tall towers in cities (Cannon et al. 2020; Teran et al. 2022). To quantify this risk, and to guide engineering design, the National Building Code of Canada prescribes the "design wind speed", which is the 50-year return period annual maximum wind speed calculated using the method of moments (NRC 2015). Considering the significant changes to the 98$^{th}$ percentile wind speed in

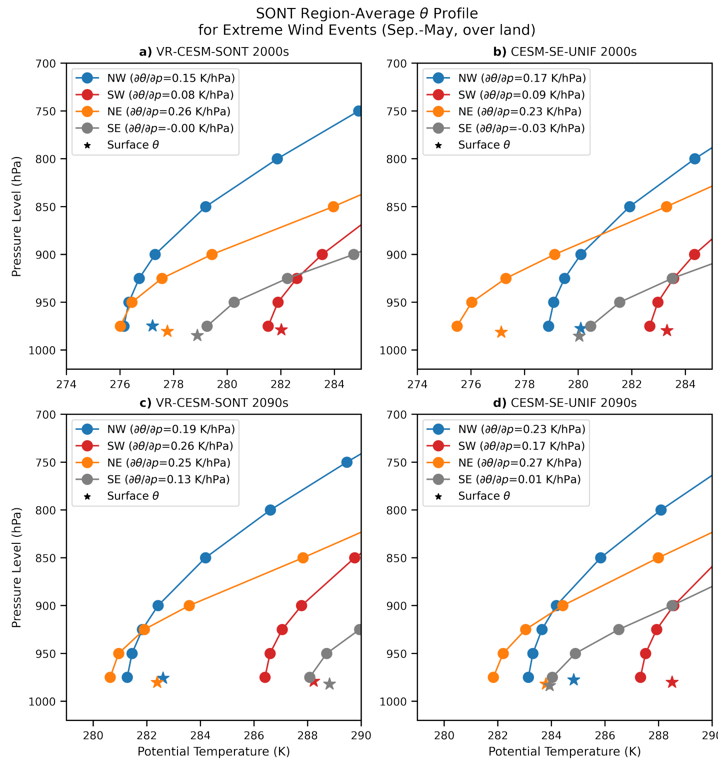


FIG. 10. Composite vertical profiles of potential temperature ($\theta$) averaged over land grid cells in the study region. Dots represent $\theta$ calculated using temperature on model levels and then interpolated onto common pressure levels for each case. Stars indicate $\theta$ calculated using surface temperature and surface pressure. Gradients of $\theta$ with respect to pressure, provided in the legends, are calculated between the surface and lowest model level. Note the different x-axis scale for the 2000s (a, b) and 2090s (c,d) cases.

each simulation, we may expect there to be significant changes to $U50$ as well. While this is the case for CESM-SE-UNIF (Fig. 11d), VR-CESM-SONT does not show the same significant increases to $U50$ (Fig. 11c) as it does $U_{98p}$, despite the magnitude of the percent changes being larger for $U50$. While it is possible that the non-significant signal in VR-CESM-SONT is due to the limited sample of 30 annual maxima, the lack of the robust land-lake contrast in the spatial pattern of the response indicates that there may not be a substantial effect on the design wind speed, despite the increase to $U_{98p}$. In other words, VR-CESM-SONT projects significantly increasing frequency and intensity of strong wind speeds, and larger yet non-significant increases to the most intense winds. The magnitude of the decreases in CESM-SE-UNIF is sufficiently large that the changes are significant, possibly in spite of the limited sampling. The decreases to $U50$ for CESM-SE-UNIF

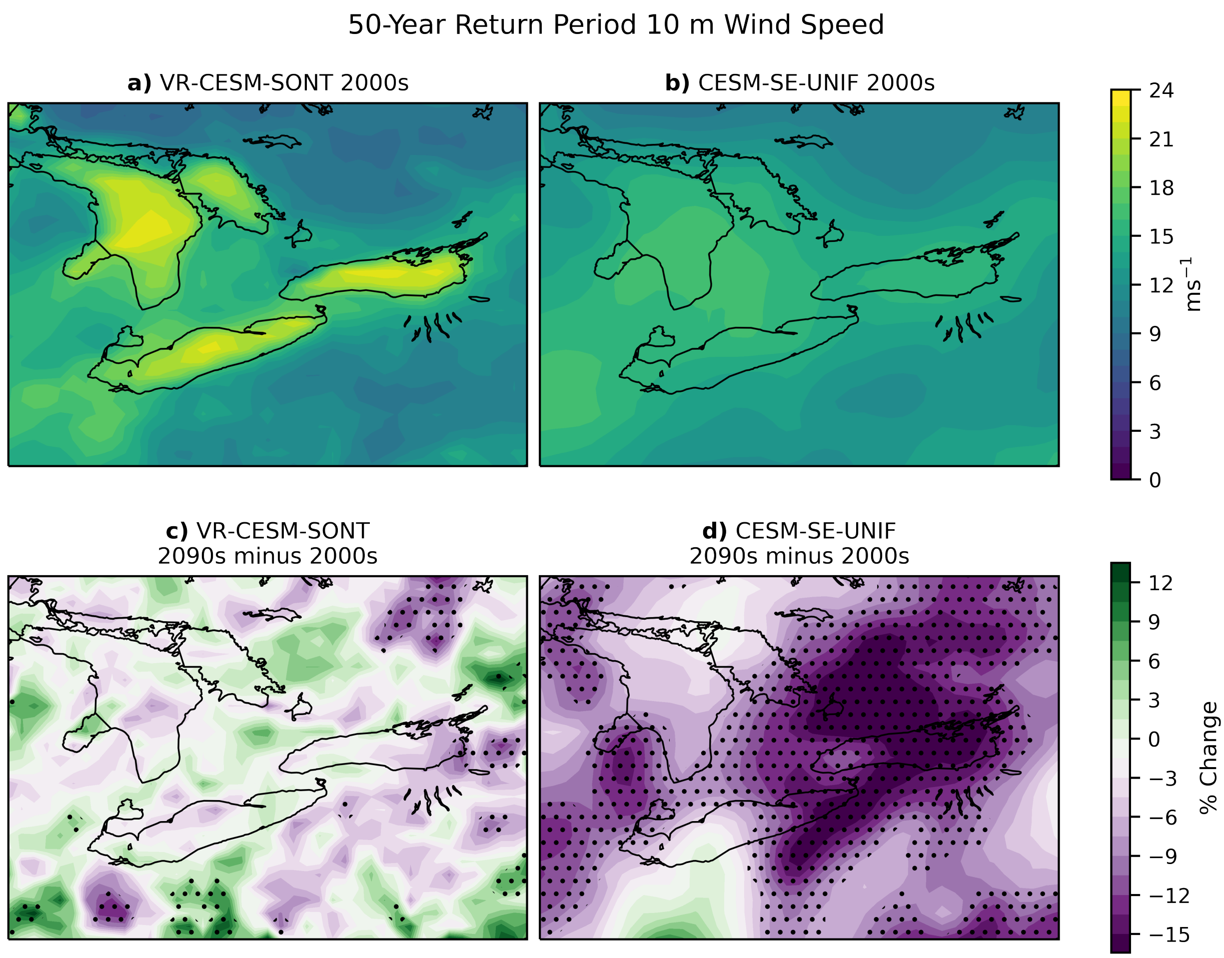


FIG. 11. (a)-(b): 50-year return period wind speeds from the 2000s forcing simulations for VR-CESM-SONT and CESM-SE-UNIF respectively. (c)-(d): Percentage changes to the 50-year return period wind speed from the 2000s to the 2090s under RCP8.5 forcing. Stippling indicates where the climate change response is statistically significant at the 10% level, based on the bootstrap resampling method described in Section 2.b.3.

over most of the study domain and are also of larger magnitude than its projected decreases to $U_{98p}$, sometimes exceeding 15%. However, these projections must be interpreted with caution, given that CESM-SE-UNIF does not adequately simulate changes relating to boundary layer stability and turbulence. Statistical significance indicates that the changes are substantial in the context of the model's climate, but the process understanding gleaned from the results of Section 3.b.3 casts doubt on the credibility of the CESM-SE-UNIF projections.

*c. Stagnant Wind Events*

Figure 3 showed that both the coarse and regionally refined resolution models project increasing frequency of extreme weak wind events, defined here as events in the bottom 5 percentiles of the wind speed distribution (Sections 2.b.1 and 2.b.2). In this section we investigate changes to 10 m wind speed during stagnant wind events, potential synoptic scale and local-scale drivers of these events, and potential human health-related impacts.

Figures 12(a) and (d) show composite changes to 10 m wind speed for stagnant wind events in the study region. Both show significant weakening over land, consistent with a reduction in the 5$^{th}$ percentile wind speed threshold. Like for extreme high wind speeds, VR-CESM-SONT shows some evidence of land-lake contrast in the sign of the projected changes — the 5$^{th}$ percentile wind speed increases significantly over part of Lake Erie and non-significantly over Lake Huron. The changes in both models are linked to increasing static stability, and the increases to 10 m wind speed occur mainly where changes to stability are weaker. In this regard, the coarse and fine resolution models are consistent in their projections of stagnant winds under climate change.

No large-scale ridge pattern (indicative of blocking) is evident in the 300 hPa wind composites for either period in either model configuration, nor lower in the atmosphere at 700 hPa (not shown). Panels (c) and (f) of Figure 12 show the composite changes to 300 hPa winds during stagnant wind events. While there is significant weakening of the jet above the study region, the changes are consistent with a poleward shift of the jet stream, which is true for the mean September–May change to 300 hPa winds. Therefore the weakening to stagnant wind speeds in CESM-SE-UNIF appear to be driven both by changes to local stability and by an overall decrease in the mean wind speed due to changes in the mean circulation.

The anomalously high stability during stagnant wind events in both models is related to a temperature inversion in the boundary layer. Figure 13 compares the composite region-averaged land temperature for the stagnant wind events to the climatological mean and a moist adiabatic profile. Each stagnant-wind composite shows temperature decreasing with height in the boundary layer which indicates the presence of an inversion. This is in agreement with the composite

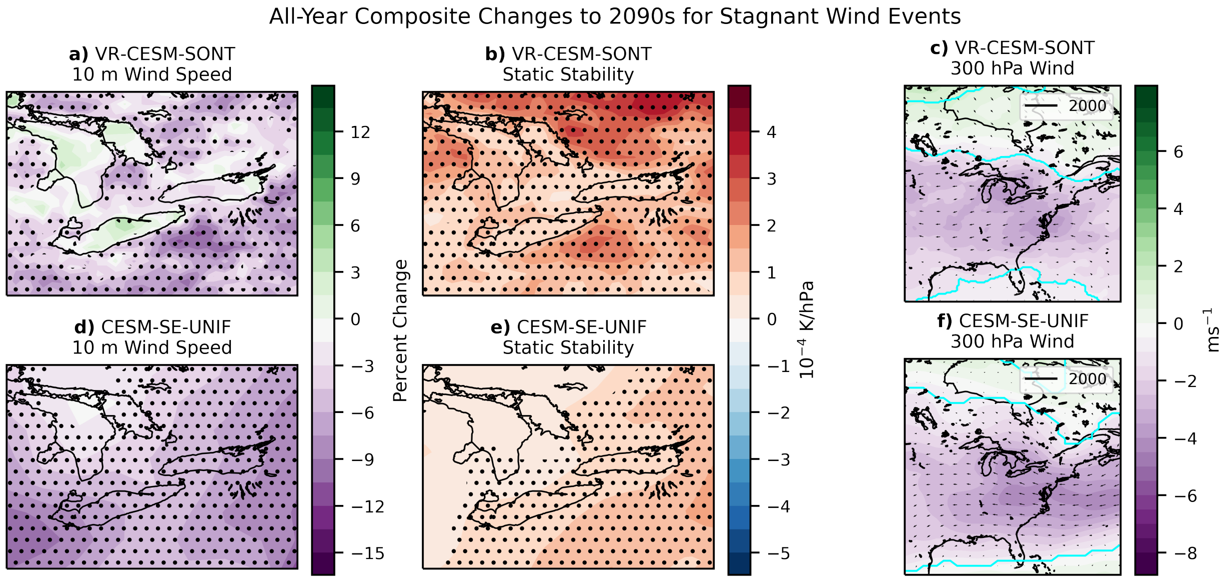


FIG. 12. Composite changes to (a), (d): 10 m wind speed (expressed as a percentage change), (b), (e): near-surface static stability, and (c), (f): 300 hPa winds for bottom-5 percentile wind speed events. Stippling in panels (a), (b), (d), and (e) indicates a statistically significant change at the 10% level, and the cyan contours in panels (c) and (f) outline regions of significant changes at the same significance level.

temperature profile for weak winds at the Buffalo radiosonde station from the Wyoming Upper Air Archive (Supplemental Figure 4). The strength of the inversion, measured by the lapse rate $\partial T/\partial p$ between the surface and lowest model level, is greater for VR-CESM-SONT and shows a minor increase under 2090s RCP8.5 forcing. The inversion strength is unchanged in the 2090s relative to the 2000s for CESM-SE-UNIF. Inversions are strongly associated with pollution and poor air quality (Dempsey 2018; Hsu and Cheng 2019), which connects increasing frequency and magnitude of stagnant winds events to harmful effects on human health.

Another potential human health related impact of stagnant winds is extreme high temperatures, particularly in urban areas (Javanroodi and Nik 2020). To investigate, we composite the daily maximum 2 m temperature anomalies for days with stagnant wind events (Fig. 14). Since extreme high temperatures, which may have effects on human health, are most commonly associated with the summer season, we include only JJA stagnant wind events in this analysis. The VR-CESM-SONT composites for both the 2000s and 2090s periods show small but significant warm anomalies

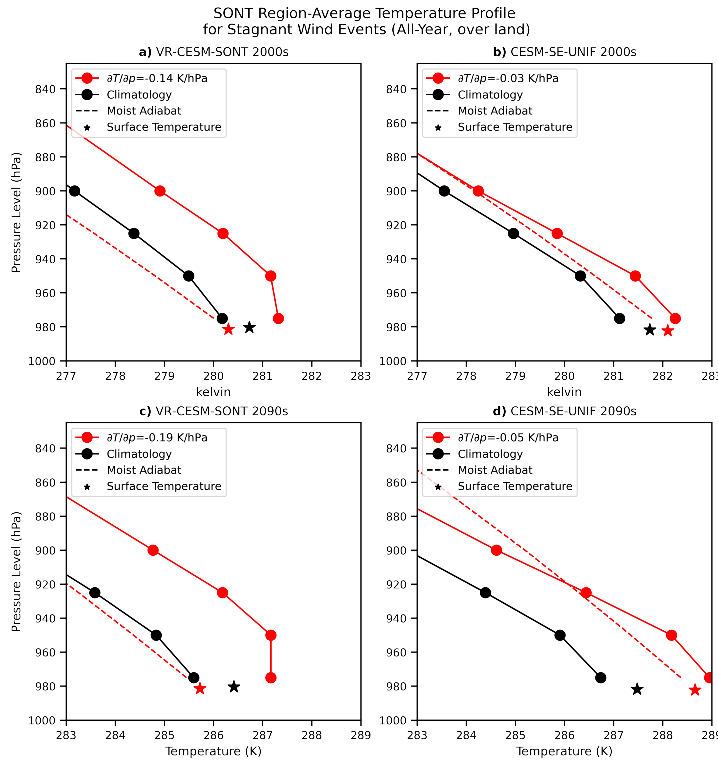


FIG. 13. Composite vertical profiles of temperature ($T$) averaged over land grid cells in the study region, for stagnant wind events (red), and the climatological mean (black). Dots represent $T$ interpolated from model levels onto common pressure levels after averaging across events. Stars indicate surface temperature and pressure. Dashed lines represent a moist adiabatic temperature profile. Gradients of $T$ with respect to pressure, provided in the legends, are calculated between the surface and lowest model level. Note the different x-axis scale for the 2000s (a, b) and 2090s (c,d) cases.

in the Great Lakes region during the stagnant wind events, confirming the association between stagnant winds and warm temperatures. Despite the anomalies being similar in magnitude for both periods, the absolute temperatures during the 2090s events are higher than for the 2000s due to overall mean warming. However, these anomalies are only on the order of 1–2°C, and are thus cannot be considered extreme high temperatures, only anomalously warm. Neither composite for CESM-SE-UNIF shows a significant warm anomaly directly in the study region near Lakes Ontario and Huron. Therefore despite CESM-SE-UNIF projecting the increasing severity of stagnant wind events, its coarse spatial resolution does not permit it to represent the temperature related impacts of these events. Composites for both model configurations and both forcing periods show a

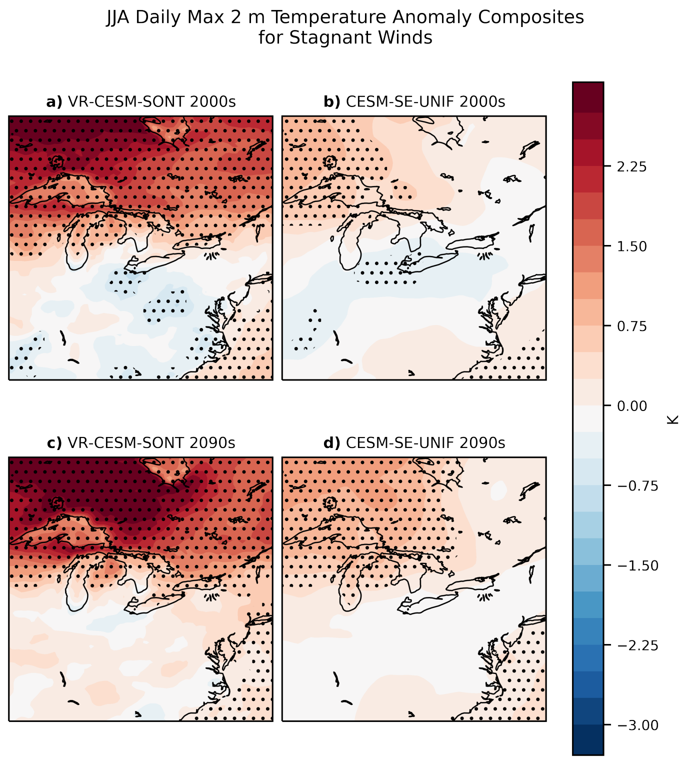


FIG. 14. Composites of anomalous daily maximum 2 m temperature for summertime (JJA) stagnant wind events in the VR-CESM-SONT and CESM-SE-UNIF 2000s-forcing simulations (a, b), and 2090s forcing simulations (c, d). Stippling indicates where anomalies deviate significantly from the seasonal mean, as described in Section 2.b.3.

significant warm anomaly to the west of the Great Lakes region. This is likely a product of warm air advection from an anticyclone centred near the study region (Supplemental Figure 5), and is thus only indirectly linked to the stagnant winds.

## 4. Conclusions

This study investigated projected changes to extreme high and low wind speeds in the eastern Great Lakes region under end-of-century RCP8.5 forcing. Each type of extreme event has important societal impacts, including damage to infrastructure for strong winds, and negative effects on human health for stagnant winds. Changes to extreme wind speeds under climate change are relatively understudied, relative to other types of extreme weather such as high temperatures and heavy precipitation (Pryor and Hahmann 2019). As such, this work addresses an important gap in extreme weather research.

Our results show that projections of extreme high wind speeds over land differ in sign between uniform coarse resolution and regionally refined resolution grids, all else being equal between the two sets of simulations. The fine-resolution simulations project statistically significant increases of 3-5% to $U_{98p}$ over land, and decreases of similar magnitude over the lakes. The coarse-resolution simulations project decreasing $U_{98p}$ nearly everywhere in the study region. The weakening of extreme high wind speeds in CESM-SE-UNIF is consistent with its projected weakening to large-scale circulation anomalies during extreme high wind events, such as ETCs and upper-level jet streaks. Similar large-scale changes are present in VR-CESM-SONT, so its $U_{98p}$ projections are not controlled by changes to large-scale circulation, but rather local-scale changes to boundary layer processes. Increasing surface heat flux destabilizes the boundary layer and enhances mixing of higher-momentum air from the lower troposphere towards the surface, strengthening extreme high wind speeds (Mioduszewski et al. 2018). The increases to surface heat flux are also present in the coarse resolution model, but without the advantage of high spatial resolution, the model is not able to resolve the corresponding increases to turbulence and strong wind speeds. A limitation of this work is that VR-CESM is a hydrostatic, non-convection-permitting model, and thus does not explicitly resolve boundary layer turbulence despite its high spatial resolution. Nevertheless, the high pattern correlations between the changes to sensible heat flux, static stability, turbulent vertical velocity, and wind speed support that this is the mechanism responsible for strengthening extreme high wind speeds. The changes to sensible heat flux are driven by changes to surface temperature, which is better understood and more robust than changes to atmospheric circulation, giving greater credibility to the VR-CESM projections than the coarse resolution projections.

Despite projecting increases to $U_{98p}$ over land, VR-CESM-SONT does not project statistically significant increases to the the 50-year return period wind speed, or “design wind speed”, over most of the study domain. It’s possible that these very-rare, very intense events are not well characterized by the 30-year sample, but at face value the results indicate that the fine-resolution model projects no robust change to the strongest wind extremes, which are most relevant for engineering design. Consistent with its projections of $U_{98p}$, the coarse resolution model projects a reductions to the design wind speed up to and exceeding 15%, indicating substantially reduced wind hazards. However, since this model is not able to resolve the effect of boundary layer turbulence on extreme winds as well as VR-CESM-SONT, these projections must also be taken with caution and merit further study. In particular, our concern is that the effects of weakening of circulation anomalies at the synoptic scale are artificially dominating the signal over the boundary layer induced strengthening at the refined scale.

Both the regionally-refined and coarse-grid simulations project increasing frequency of extreme stagnant wind speeds. These events are associated with temperature inversions that trap pollutants and lead to poor air quality (Dempsey 2018). The literature has also linked stagnant winds with extreme high temperatures in urban regions (Javanroodi and Nik 2020). VR-CESM-SONT shows significant warm anomalies during summer season stagnant wind events, but neither model shows evidence of extreme high temperatures. Both models agree that reduced static stability is a mechanism for the changes to stagnant winds, but only the high resolution model is capable of resolving the impacts of stagnant wind events, namely inversions and anomalously high summertime temperatures.

Several previous studies (Najac et al. 2011; Cheng et al. 2012; Pryor et al. 2012; Pryor and Barthelmie 2014; Jeong and Sushama 2019), have investigated dynamically and/or statistically downscaled projections of extreme wind speeds under climate change, but few focus on the dynamical processes causing the changes. By identifying physical mechanisms responsible for the changes to extreme high and low wind speeds, we build confidence in the projections of VR-CESM. Planned future research will involve investigation of changes to extreme wind speeds and their mechanisms using VR-CESM with refined grids centred on additional regions. Extreme wind speeds and their drivers are highly region-dependent (Jeong and Sushama 2019), so additional work is needed to characterize changes to extreme winds outside of the Great Lakes region. For example, the wind climate in the Rocky Mountains is strongly influenced by topographic forcing (Sherry and Rival 2015), which is better represented with the regionally-refined resolution of VR-CESM (Zarzycki et al. 2015). Investigation of the robustness of the land-water contrast in projections of extreme high winds could be performed using refined grids covering coastal North America, or other regions where the climate is influenced by large lakes such as the African Great Lakes. Further robustness of our results could be examined by considering additional high-resolution climate models, including both RCM and HighResMIP (Haarsma et al. 2016) simulations.

*Acknowledgments.* The authors acknowledge funding from the Natural Sciences and Engineering Research Council of Canada (NSERC Discovery Grants RGPIN-2019-05406 and RGPIN-2020-06204), the Centre for Climate Science and Engineering at the University of Toronto (Dean's Strategic Fund DSF 18-30), Climate Positive Energy, and the Ontario Graduate Scholarship. Computations were performed on the Niagara supercomputer at the SciNet HPC Consortium. SciNet is funded by the Canada Foundation for Innovation; the Government of Ontario; Ontario Research Fund–Research Excellence; and the University of Toronto. This material is based in part on work supported by the National Center for Atmospheric Research (NCAR), which is a major facility sponsored by the National Science Foundation (NSF) and managed by the University Corporation for Atmospheric Research. The CESM project is supported primarily by the NSF.

*Data availability statement.* Post-processed output from the VR-CESM-SONT and CESM-SE-UNIF simulations, required to reproduce the figures, and the SCRIP and EXODUS files for the variable resolution grid, are archived at `https://doi.org/10.5683/SP3/WZ6QGE`. Radiosonde data was retrieved from the Wyoming Upper Air Archive (`https://weather.uwyo.edu/upperair/sounding.html`) using the Siphon Python package (May et al. 2017). ERA5 reanalysis data (Hersbach et al. 2020) was retrieved from the Copernicus Climate Data Store (`https://doi.org/10.24381/cds.adbb2d47`).

## References

Ashley, W. S., and A. W. Black, 2008: Fatalities Associated with Nonconvective High-Wind Events in the United States. *Journal of Applied Meteorology and Climatology*, **47 (2)**, 717–725, https://doi.org/10.1175/2007JAMC1689.1.

Bretherton, C. S., and S. Park, 2009: A New Moist Turbulence Parameterization in the Community Atmosphere Model. *Journal of Climate*, **22 (12)**, 3422–3448, https://doi.org/10.1175/2008JCLI2556.1.

Burakowski, E. A., A. Tawfik, A. Ouimette, L. Lepine, C. Zarzycki, K. Novick, S. Ollinger, and G. Bonan, 2019: Simulating surface energy fluxes using the variable-resolution Community Earth System Model (VR-CESM). *Theor Appl Climatol*, **138 (1-2)**, 115–133, https://doi.org/10.1007/s00704-019-02785-0.

Cannon, A. J., D. I. Jong, X. Zhang, and F. W. Zwiers, 2020: Climate-resilient buildings and core public infrastructure 2020 : an assessment of the impact of climate change on climatic design data in Canada. URL https://publications.gc.ca/site/eng/9.893021/publication.html, last Modified: 2013-04-03.

Cheng, C. S., G. Li, Q. Li, H. Auld, and C. Fu, 2012: Possible Impacts of Climate Change on Wind Gusts under Downscaled Future Climate Conditions over Ontario, Canada. *J. Climate*, **25 (9)**, 3390–3408, https://doi.org/10.1175/JCLI-D-11-00198.1.

CSEG, 2013: CESM1.2 Release Series User's Guide. National Center for Atmospheric Research, URL https://www2.cesm.ucar.edu/models/cesm1.2/cesm/doc_cesm1_2_1/usersguide/ug.pdf.

Dempsey, F., 2018: A Survey of Regional-Scale Blocking Patterns and Effects on Air Quality in Ontario, Canada. *Atmosphere*, **9 (6)**, 226, https://doi.org/10.3390/atmos9060226.

Dennis, J. M., and Coauthors, 2012: CAM-SE: A scalable spectral element dynamical core for the Community Atmosphere Model. *The International Journal of High Performance Computing Applications*, **26 (1)**, 74–89, https://doi.org/10.1177/1094342011428142.

Garrido-Perez, J. M., C. Ordóñez, R. García-Herrera, and D. Barriopedro, 2018: Air stagnation in Europe: Spatiotemporal variability and impact on air quality. *Science of The Total Environment*, **645**, 1238–1252, https://doi.org/10.1016/j.scitotenv.2018.07.238.

Gettelman, A., P. Callaghan, V. E. Larson, C. M. Zarzycki, J. T. Bacmeister, P. H. Lauritzen, P. A. Bogenschutz, and R. B. Neale, 2018: Regional Climate Simulations With the Community Earth System Model. *Journal of Advances in Modeling Earth Systems*, **10 (6)**, 1245–1265, https://doi.org/10.1002/2017MS001227.

Haarsma, R. J., and Coauthors, 2016: High Resolution Model Intercomparison Project (HighResMIP v1.0) for CMIP6. *Geosci. Model Dev.*, **9 (11)**, 4185–4208, https://doi.org/10.5194/gmd-9-4185-2016.

Hanley, J., and R. Caballero, 2012: The role of large-scale atmospheric flow and Rossby wave breaking in the evolution of extreme windstorms over Europe. *Geophysical Research Letters*, **39 (21)**, https://doi.org/10.1029/2012GL053408.

Hersbach, H., and Coauthors, 2020: The ERA5 global reanalysis. *Q.J.R. Meteorol. Soc.*, **146 (730)**, 1999–2049, https://doi.org/10.1002/qj.3803.

Hsu, C.-H., and F.-Y. Cheng, 2019: Synoptic Weather Patterns and Associated Air Pollution in Taiwan. *Aerosol Air Qual. Res.*, **19 (5)**, 1139–1151, https://doi.org/10.4209/aaqr.2018.09.0348.

Hurrell, J. W., and Coauthors, 2013: The Community Earth System Model: A Framework for Collaborative Research. *Bulletin of the American Meteorological Society*, **94 (9)**, 1339–1360, https://doi.org/10.1175/BAMS-D-12-00121.1.

Jabbari, A., J. D. Ackerman, L. Boegman, and Y. Zhao, 2021: Increases in Great Lake winds and extreme events facilitate interbasin coupling and reduce water quality in Lake Erie. *Sci Rep*, **11 (1)**, 5733, https://doi.org/10.1038/s41598-021-84961-9.

Javanroodi, K., and V. M. Nik, 2020: Interactions between extreme climate and urban morphology: Investigating the evolution of extreme wind speeds from mesoscale to microscale. *Urban Climate*, **31**, 100 544, https://doi.org/10.1016/j.uclim.2019.100544.

Jeong, D. I., and L. Sushama, 2019: Projected Changes to Mean and Extreme Surface Wind Speeds for North America Based on Regional Climate Model Simulations. *Atmosphere*, **10 (9)**, 497, https://doi.org/10.3390/atmos10090497.

Kay, J. E., and Coauthors, 2015: The Community Earth System Model (CESM) Large Ensemble Project: A Community Resource for Studying Climate Change in the Presence of Internal Climate Variability. *Bulletin of the American Meteorological Society*, **96 (8)**, 1333–1349, https://doi.org/10.1175/BAMS-D-13-00255.1.

Larsén, X. G., S. Ott, J. Badger, A. N. Hahmann, and J. Mann, 2012: Recipes for Correcting the Impact of Effective Mesoscale Resolution on the Estimation of Extreme Winds. *Journal of Applied Meteorology and Climatology*, **51 (3)**, 521–533, https://doi.org/10.1175/JAMC-D-11-090.1.

Lawrence, D. M., and Coauthors, 2019: The Community Land Model Version 5: Description of New Features, Benchmarking, and Impact of Forcing Uncertainty. *J Adv Model Earth Syst*, **11 (12)**, 4245–4287, https://doi.org/10.1029/2018MS001583.

Letson, F. W., R. J. Barthelmie, K. I. Hodges, and S. C. Pryor, 2021: Intense windstorms in the northeastern United States. *Nat. Hazards Earth Syst. Sci.*, **21 (7)**, 2001–2020, https://doi.org/10.5194/nhess-21-2001-2021.

Loken, C., and Coauthors, 2010: SciNet: Lessons Learned from Building a Power-efficient Top-20 System and Data Centre. *J. Phys.: Conf. Ser.*, **256**, 012 026, https://doi.org/10.1088/1742-6596/256/1/012026.

Lukens, K. E., E. H. Berbery, and K. I. Hodges, 2018: The Imprint of Strong-Storm Tracks on Winter Weather in North America. *J. Climate*, **31 (5)**, 2057–2074, https://doi.org/10.1175/JCLI-D-17-0420.1.

May, R., S. Arms, J. Leeman, and J. Chastang, 2017: Siphon: A collection of Python utilities for accessing remote atmospheric and oceanic datasets. Boulder, Colorado, URL https://github.com/Unidata/siphon, https://doi.org/10.5065/D6CN72NW.

McVicar, T. R., and Coauthors, 2012: Global review and synthesis of trends in observed terrestrial near-surface wind speeds: Implications for evaporation. *Journal of Hydrology*, **416-417**, 182–205, https://doi.org/10.1016/j.jhydrol.2011.10.024.

Mioduszewski, J., S. Vavrus, and M. Wang, 2018: Diminishing Arctic Sea Ice Promotes Stronger Surface Winds. *J. Climate*, **31 (19)**, 8101–8119, https://doi.org/10.1175/JCLI-D-18-0109.1.

Morris, M., P. J. Kushner, G. W. K. Moore, and O. Mercan, 2023: Atmospheric Circulation Patterns Associated with Extreme Wind Events in Canadian Cities. *Journal of Climate*, **36 (13)**, 4443–4460, https://doi.org/10.1175/JCLI-D-22-0719.1.

Najac, J., C. Lac, and L. Terray, 2011: Impact of climate change on surface winds in France using a statistical-dynamical downscaling method with mesoscale modelling: IMPACT OF CLIMATE CHANGE ON SURFACE WINDS IN FRANCE. *Int. J. Climatol.*, **31 (3)**, 415–430, https://doi.org/10.1002/joc.2075.

Neale, R. B., and Coauthors, 2012: Description of the NCAR Community Atmosphere Model (CAM 5.0). Tech. rep., National Center for Atmospheric Research, 289 pp.

NRC, 2015: National Building Code of Canada: 2015 - NRC Publications Archive. URL https://nrc-publications.canada.ca/eng/view/object/?id=c8876272-9028-4358-9b42-6974ba258d99.

Ponce, M., and Coauthors, 2019: Deploying a Top-100 Supercomputer for Large Parallel Workloads: the Niagara Supercomputer. *Proceedings of the Practice and Experience in Advanced Research Computing on Rise of the Machines (learning)*, Association for Computing Machinery, New York, NY, USA, 1–8, PEARC '19, https://doi.org/10.1145/3332186.3332195, URL https://doi.org/10.1145/3332186.3332195.

Priestley, M. D. K., and J. L. Catto, 2022: Future changes in the extratropical storm tracks and cyclone intensity, wind speed, and structure. *Weather Clim. Dynam.*, **3 (1)**, 337–360, https://doi.org/10.5194/wcd-3-337-2022.

Pryor, S., and A. Hahmann, 2019: Downscaling Wind. *Oxford Research Encyclopedia of Climate Science*, Oxford University Press, https://doi.org/10.1093/acrefore/9780190228620.013.730, URL http://oxfordre.com/climatescience/view/10.1093/acrefore/9780190228620.001.0001/acrefore-9780190228620-e-730.

Pryor, S. C., and R. J. Barthelmie, 2014: Hybrid downscaling of wind climates over the eastern USA. *Environ. Res. Lett.*, **9 (2)**, 024 013, https://doi.org/10.1088/1748-9326/9/2/024013.

Pryor, S. C., R. J. Barthelmie, M. S. Bukovsky, L. R. Leung, and K. Sakaguchi, 2020: Climate change impacts on wind power generation. *Nat Rev Earth Environ*, **1 (12)**, 627–643, https://doi.org/10.1038/s43017-020-0101-7.

Pryor, S. C., R. J. Barthelmie, and J. T. Schoof, 2012: Past and future wind climates over the contiguous USA based on the North American Regional Climate Change Assessment Program model suite: NARCCAP WIND CLIMATES. *J. Geophys. Res.*, **117 (D19)**, n/a–n/a, https://doi.org/10.1029/2012JD017449.

Sandink, D., G. Kopp, S. Stevenson, and N. Dale, 2019: Increasing High Wind Safety for Canadian Homes: A Foundational Document for Low-Rise Residential and Small Buildings. *ICLR Research Paper Series*, **62**, 128.

Schuldt, S. J., M. R. Nicholson, Y. A. Adams, and J. D. Delorit, 2021: Weather-Related Construction Delays in a Changing Climate: A Systematic State-of-the-Art Review. *Sustainability*, **13 (5)**, 2861, https://doi.org/10.3390/su13052861.

Scinocca, J. F., and Coauthors, 2016: Coordinated Global and Regional Climate Modeling. *Journal of Climate*, **29 (1)**, 17–35, https://doi.org/10.1175/JCLI-D-15-0161.1.

Seneviratne, S. I., and Coauthors, 2023: Weather and Climate Extreme Events in a Changing Climate. *Climate Change 2021 – The Physical Science Basis: Working Group I Contribution to the Sixth Assessment Report of the Intergovernmental Panel on Climate Change*, 1st ed., Cambridge University Press, https://doi.org/10.1017/9781009157896, URL https://www.cambridge.org/core/product/identifier/9781009157896/type/book.

Shaw, T. A., and Coauthors, 2016: Storm track processes and the opposing influences of climate change. *Nature Geosci*, **9 (9)**, 656–664, https://doi.org/10.1038/ngeo2783.

Sherry, M., and D. Rival, 2015: Meteorological phenomena associated with wind-power ramps downwind of mountainous terrain. *Journal of Renewable and Sustainable Energy*, **7 (3)**, 033 101, https://doi.org/10.1063/1.4919021.

Sillmann, J., and Coauthors, 2017: Understanding, modeling and predicting weather and climate extremes: Challenges and opportunities. *Weather and Climate Extremes*, **18**, 65–74, https://doi.org/10.1016/j.wace.2017.10.003.

Sinclair, V. A., M. Rantanen, P. Haapanala, J. Räisänen, and H. Järvinen, 2020: The characteristics and structure of extra-tropical cyclones in a warmer climate. *Weather Clim. Dynam.*, **1 (1)**, 1–25, https://doi.org/10.5194/wcd-1-1-2020.

Skamarock, W. C., 2004: Evaluating Mesoscale NWP Models Using Kinetic Energy Spectra. *Mon. Wea. Rev.*, **132 (12)**, 3019–3032, https://doi.org/10.1175/MWR2830.1.

Teran, A. S., and Coauthors, 2022: Towards a Computational Workflow for Studying the Effects of Climate Change on Wind Loads on High-Rise Buildings in Urban Areas. *Atmosphere-Ocean*, **60 (2)**, 124–140, https://doi.org/10.1080/07055900.2022.2061412.

Trier, S. B., R. D. Sharman, D. Muñoz-Esparza, and T. P. Lane, 2020: Environment and Mechanisms of Severe Turbulence in a Midlatitude Cyclone. *Journal of the Atmospheric Sciences*, **77 (11)**, 3869–3889, https://doi.org/10.1175/JAS-D-20-0095.1.

Uccellini, L. W., and P. J. Kocin, 1987: The Interaction of Jet Streak Circulations during Heavy Snow Events along the East Coast of the United States. *Wea. Forecasting*, **2 (4)**, 289–308, https://doi.org/10.1175/1520-0434(1987)002⟨0289:TIOJSC⟩2.0.CO;2.

US EPA, R. ., 2015: Facts and Figures about the Great Lakes. URL https://www.epa.gov/greatlakes/facts-and-figures-about-great-lakes, archive Location: Great Lakes.

Wang, M., P. Ullrich, and D. Millstein, 2018: The future of wind energy in California: Future projections with the Variable-Resolution CESM. *Renewable Energy*, **127**, 242–257, https://doi.org/10.1016/j.renene.2018.04.031.

Wang, M., P. Ullrich, and D. Millstein, 2020: Future projections of wind patterns in California with the variable-resolution CESM: a clustering analysis approach. *Clim Dyn*, **54 (3)**, 2511–2531, https://doi.org/10.1007/s00382-020-05125-5.

Welch, B. L., 1938: The Significance of the Difference Between Two Means when the Population Variances are Unequal. *Biometrika*, **29 (3/4)**, 350–362, https://doi.org/https://doi.org/10.2307/2332010.

Welker, C., and O. Martius, 2015: Large-scale atmospheric flow conditions and sea surface temperatures associated with hazardous winds in Switzerland. *Clim Dyn*, **44 (7-8)**, 1857–1869, https://doi.org/10.1007/s00382-014-2404-1.

Wilks, D. S., 2016: “The Stippling Shows Statistically Significant Grid Points”: How Research Results are Routinely Overstated and Overinterpreted, and What to Do about It. *Bulletin of the American Meteorological Society*, **97 (12)**, 2263–2273, https://doi.org/10.1175/BAMS-D-15-00267.1.

Zarzycki, C. M., C. Jablonowski, D. R. Thatcher, and M. A. Taylor, 2015: Effects of Localized Grid Refinement on the General Circulation and Climatology in the Community Atmosphere Model. *Journal of Climate*, **28 (7)**, 2777–2803, https://doi.org/10.1175/JCLI-D-14-00599.1.

Zeng, Z., and Coauthors, 2019: A reversal in global terrestrial stilling and its implications for wind energy production. *Nat. Clim. Chang.*, **9 (12)**, 979–985, https://doi.org/10.1038/s41558-019-0622-6.

Zha, J., and Coauthors, 2021: Projected changes in global terrestrial near-surface wind speed in 1.5 °C–4.0 °C global warming levels. *Environ. Res. Lett.*, **16 (11)**, 114 016, https://doi.org/10.1088/1748-9326/ac2fdd.